Globular Cluster Photometry with the Hubble Space Telescope. VI. WF/PC-I Observations of the Stellar Populations in the Core of M13 (NGC 6205)

Randi L. Cohen and Puragra Guhathakurta
UCO/Lick Observatory, University of California, Santa Cruz, CA 95064, USA
Email: randi@ucolick.org, raja@ucolick.org

Brian Yanny
Fermi National Accelerator Laboratory, Batavia, IL 60510, USA
Email: yanny@sdss.fnal.gov

Donald P. Schneider
Department of Astronomy & Astrophysics, The Pennsylvania State University, University Park, PA 16802, USA
Email: dps@astro.psu.edu

John N. Bahcall
Institute for Advanced Study, Princeton, NJ 08540, USA
Email: jnb@sns.ias.edu

ABSTRACT

We study the dense core of the globular cluster Messier 13 (NGC 6205) using pre-refurbishment Planetary Camera-I images obtained with the *Hubble Space Telescope.* Short exposures (60 s) through the F555W and F785LP filters (similar to Johnson V and I, respectively) have been used to obtain V and I photometry of 2877 stars brighter than $V \sim 20$ in a 1.25 arcmin^2 region of the cluster including its core and extending out to $r \sim 66''$ (2.3 pc) from its center. The sample is complete to $V \simeq 18.3$ (the main sequence turnoff) and the 1σ photometric error is about 0.1 mag. We find 15 blue straggler star candidates and 10 other possible blue stragglers in this region of M13. Their specific frequency is in the range $F_{\rm BSS} = 0.04$–0.07, comparable to what is observed near the centers of other dense clusters. A comparison between M13's observed V band stellar luminosity function and a theoretical model (Bergbusch & Vandenberg 1992) for the luminosity function of an old, metal-poor cluster shows that the model predicts too few of the brightest red giants ($V \sim 12.5$–15) by a factor of two relative to subgiants/turnoff stars ($> 6\sigma$ effect). The radial distributions of the red giants, blue stragglers, and subgiants are consistent with one another, and are well fit by a King profile of core radius $r_{\rm core} = 38'' \pm 6''$ (90% confidence limits) or 1.3 pc. Stars in the blue horizontal branch of M13, however, appear to be centrally depleted relative to other stellar types.

We combine data from three dense 'King model clusters', M13, M3, and 47 Tuc, and two post core collapse clusters, M30 and M15, and compare the distributions of various stellar types as a function of $(r/r_{\rm half\ light})$ and $(r/r_{\rm core})$. The horizontal branch stars in the combined sample appear to be centrally depleted relative to the giants (97% significance)—this depletion is only a 1σ–2σ effect in each of the clusters taken individually. The blue stragglers in the combined sample are centrally concentrated relative to the giants.

Subject headings: cluster: globular – stars: blue straggler – stars: blue horizontal branch – stars: luminosity function – cluster: M13 (NGC 6205)

1. INTRODUCTION

This is the sixth in a series of papers describing *Hubble Space Telescope* (*HST*) observations of the centers of the nearest Galactic globular clusters with $|b| > 15°$. The main scientific goals of this program are to measure the shape of stellar density profile in clusters and to understand the nature of evolved stellar populations in very dense regions by probing the variation in the mix of stellar types as a function of radius (and hence stellar density). In this paper, we apply the techniques developed in our earlier Planetary Camera-I (PC) studies of 47 Tuc (Guhathakurta et al. 1992, hereafter referred to as Paper I) and M15 (Yanny et al. 1994a, hereafter referred to as Paper II) to analyze data on M13 (NGC 6205).

The globular cluster M13 is the least dense of the clusters analyzed thus far in this series of papers: M3, 47 Tuc, M30, and M15. The core of M13 has a projected stellar density of ~ 0.3 arcsec^{-2} (300 pc^{-2}) for stars with $V < V_{\rm HB} + 2$. [The easy detectability of this sample of bright stars (upto 2 mag fainter than the horizontal branch) makes it a convenient tracer of the relative surface density of clusters (Bolte et al. 1993).] By contrast, the density of M3's core is ~ 1.1 arcsec^{-2} (460 pc^{-2}), the density of 47 Tuc's core is ~ 3 arcsec^{-2} (6000 pc^{-2}), and the density in the central few arcseconds of M15 and M30 exceeds 30 arcsec^{-2} ($> 10^4$ pc^{-2}). Thus, the effect of crowding on the completeness and photometric accuracy of our M13 sample is less severe than in our earlier PC studies.

The total absolute visual magnitude of M13 is $M_V = -8.51$, based on an estimated distance of 7.2 kpc (Djorgovski 1993). The cluster has a metallicity of [Fe/H] $= -1.65$

(Djorgovski 1993) and has an extended blue horizontal branch. In fact, M13's horizontal branch is entirely on the blue side of the RR Lyrae instability strip and is significantly bluer than the horizontal branches of other clusters of comparable metallicity (M3 and NGC 7006), making it important in the search for the (unknown) second parameter that is thought to control horizontal branch morphology in globular clusters (Zinn 1986). The surface brightness profile of M13 is well fit by a King profile with a core of radius $r_{\rm core} = 53'' \pm 7''$ or 1.8 pc (Trager et al. 1993). The cluster displays a significant amount of rotation with a maximum rotation speed of about $5\,{\rm km\ s^{-1}}$ (Lupton et al. 1987).

Its relative proximity to the Sun and large size have made M13 the subject of several studies in the last four decades (Savedoff 1956; Baum et al. 1959; Sandage 1970; Cudworth & Monet 1979; Lupton & Gunn 1986; Laget et al. 1992; Guarnieri et al. 1993). Recently, Stetson (1996) derived an accurate color–magnitude diagram of stars located just outside the cluster core using images obtained with the Canada–France–Hawaii telescope. Our *HST* investigation of M13's core is complementary to Stetson's study. Despite the broad and complicated wings of the pre-refurbishment *HST*'s aberrated point spread function, its $0\farcs1$ (FWHM) core makes it possible to detect faint stars in crowded fields. Pre-refurbishment *HST* data yield cleaner and more complete stellar samples in dense globular cluster cores than even $0\farcs5$-seeing ground-based images (cf. Bolte et al. 1993; Guhathakurta et al. 1994, hereafter referred to as Paper III).

In Sec. 2, we describe the acquisition and processing of the *HST* PC data used in this study. In Sec. 3, we present a color–magnitude diagram of post main sequence stars in M13's core, study the relative radial distributions of the different evolved stellar populations in M13 and in two other dense clusters, and compare M13's stellar luminosity function to a theoretical luminosity function. The conclusions of the paper are summarized in Sec. 4.

2. THE DATA

2.1. Observations

Two 60 s exposures of M13 were obtained in January 1991 with *HST*'s Planetary Camera-I, one through each of the F555W and F785LP filters. These bandpasses are roughly similar to the Johnson V and I bands, respectively (Harris et al. 1991). Each PC image consists of a 2×2 mosaic of 800×800 CCD images (PC5–PC8) with a pixel scale of about $0\farcs044$. A greyscale representation of the F555W mosaic image of M13 is shown in Figure 1. The field of view of the CCD mosaic image is $68'' \times 68''$ with $\sim 0\farcs5$-wide unusable strips between adjacent CCD frames. The telescope was pointed so that the center of the cluster was imaged on PC6; the pointing was identical for the F555W and F785LP exposures. The gain of the PC CCDs is 7.6 electrons ADU^{-1} and the read noise is about 13 electrons. The limited dynamic range of the analog-to-digital converters results in saturation of the raw CCD frames at the level of 4096 ADU (3×10^4 electrons). Details of the instrument may be found in Griffiths (1989), Burrows et al. (1991), and Faber (1992); see Paper I for details of the instrumental configuration used for these observations.

2.2. Data Processing

The images were processed via the standard Space Telescope Science Institute pipeline, the primary elements of which were overscan correction, bias ("zero") subtraction, analog-to-digital bit correction, and flat fielding (Lauer 1989). Bad columns were visually identified and interpolated over. Bias subtraction and flat fielding lower the saturation level to ~ 3500 ADU and cause the saturation level to vary by $\lesssim 10\%$ across the image. At most 5 pixels at the centers of the point spread function (PSF) cores of the brightest stars in the F555W image ($V \lesssim 14.5$) and at most 2 pixels at the centers of the brightest stars in the F785LP image ($I \lesssim 12.2$) were saturated. Saturated pixels were masked and subsequently ignored, and only the unsaturated wings of the saturated bright stars were used in the PSF building process and in the PSF fit to derive stellar photometry (see below).

The spherical aberration of the pre-refurbishment *HST* optics produces a spatially-varying PSF with a complex shape (Fig. 1): a sharp core (FWHM = $0''.1$) contains $\sim 10\%$ of the light while the rest is distributed in a faint, but complex halo extending out to $r_{\rm PSF} \approx 2''.5$ (Burrows et al. 1991). Faint stars located within the PSF wings of bright stars are measured reliably only if the model of the PSF accurately accounts for the light in the wings of the bright star. Papers I and II describe a star-finding, PSF-building, and PSF-fitting procedure based on DAOPHOT and DAOPHOT II (Stetson 1987, 1992), designed to extract accurate stellar photometry under crowded conditions (i.e., where there is significant overlap between the PSFs of stars in the image).

The FIND routine of the DAOPHOT package, a matched filter convolution technique, was used to find stars on the F555W and F785LP images. The DAOPHOT detection list for each CCD image was manually edited to remove spurious detections (e.g., the PSF tendrils of bright stars) and to add stars fainter than the FIND threshold, based on an inspection of the residual image, the difference between the original image and the best fit PSF template (see below). The reader is referred to Papers I and II for details.

The number of bright stars in the PC image of M13 suitable for building a PSF template is small (15–20)—at least 30 bright, relatively isolated stars per CCD image are needed to reliably build a quadratic template. Because of this, it was deemed best *not* to follow the full PSF-building process described in Paper I. We instead experimented with a pre-existing set of PSF templates derived from our earlier 47 Tuc, M15, and M3 images obtained in March 1991, April 1991, and July 1992, respectively (Papers I, II, and III, respectively). Each set consists of eight quadratically variable templates (as defined in the DAOPHOT II package), one for each of CCDs PC5–PC8 and for each of the F555W and F785LP images. Each of the three pre-existing sets of PSF templates was fit to the stars in the M13 detection list using DAOPHOT II's PSF-fitting program ALLSTAR. While the photometric lists were roughly similar for the three sets of templates, the M3 PSF templates produced residual images (original minus PSF template) that were slightly smoother than those obtained with the other two sets of templates. In fact, the M13 residual image is comparable in quality to the residual images of the clusters in our earlier studies in which the PSF template was derived in an internally consistent fashion (i.e., from stellar images in the dataset).

The eight M3 PSF templates (PC5–PC8, F555W and F785LP) were used to make a simultaneous fit to all the resolved stars on the corresponding M13 PC CCD images, yielding positions and instrumental magnitudes in the process (see Paper I for details). An F555W vs F555W − F785LP color–magnitude diagram (CMD) was obtained for each of the four PC CCDs. These CMDs were used for matching the zeropoints of the F555W and F785LP instrumental magnitude scales between the four CCDs, using as reference points the brightness of the horizontal branch (HB) and the color of the red giant branch (RGB) at the level of the HB. Typical inter-CCD zeropoint adjustments amounted to $\lesssim \pm 0.05$ mag, consistent with the values found in our earlier studies (Papers I and II).

2.3. Completeness and Photometric Accuracy

The F555W simulations that we carried out for our earlier 47 Tuc study (Paper I) can be used to assess the degree of completeness and level of photometric accuracy in the M13 dataset. The difference between the apparent distance moduli of the two clusters (difference between their $V_{\rm HB}$) is $\Delta(V - M_V)_{\rm obs} \sim +0.9$ mag, with M13 being fainter. Most of this difference is attributed to the difference in their distances from the Sun [$D_{47\,\rm Tuc} = 4.6$ kpc; $D_{\rm M13} = 7.2$ kpc; $\Delta(V - M_V)_0 = +0.97$ mag], since neither cluster is appreciably reddened [$(A_V)_{47\,\rm Tuc} = 0.12$ mag; $(A_V)_{\rm M13} = 0.06$ mag]. The shape of the observed V-band stellar luminosity function (LF) of post main sequence stars is very similar for the two clusters, after one accounts for the 0.9 mag shift between their apparent V

magnitude scales. The *HST* PC exposure times, $t_{47\,\rm Tuc} = 26\,$s and $t_{\rm M13} = 60\,$s, were chosen to exactly compensate for this magnitude difference: $2.5\log(t_{\rm M13}/t_{47\,\rm Tuc}) = 0.91$ mag. Since sky noise is unimportant in these short exposures, this implies that the ratio of signal to (read) noise is practically identical for two stars of a given *absolute* V magnitude in the two clusters.

As described in Paper I, we have carried out simulations in the F555W band with a variety of projected stellar densities: 2000, 1000, and 500 simulations (these numbers refer to the approximate number of stars brighter than the main sequence turnoff within the ~ 0.3 arcmin^2 field of view of a single PC CCD). The 2000/F555W simulation mimics the stellar surface density in the core of 47 Tuc; the projected stellar density in M13's core is about an order of magnitude lower. The 1000/F555W and 500/F555W simulations indicate that the M13 F555W dataset is $> 90\%$ complete for stars with F555W < 19 (shifting the magnitude scale in Fig. 10 of Paper I by $+0.9$ mag). This is consistent with M13's observed stellar LF in the F555W band, which continues to rise to F555W ~ 19, but drops sharply due to incompleteness beyond F555W $= 20$ (Fig. 2). It is evident from Figure 2 that the magnitude at which incompleteness sets in is independent of radial distance from the cluster center; this is due to the fact that M13's core covers a large fraction of the area of the four-CCD PC mosaic so that the stellar surface density (or the degree of crowding) only varies by a factor of 4 across the PC image.

The rms photometric uncertainty in the F555W band is expected to be $1\sigma \lesssim 0.1$ mag for stars with F555W < 19, with a somewhat non-Gaussian error distribution (see Figs. 5 and 6 of Paper I). This is in rough agreement with estimates of the photometric error derived from the observed width of M13's RGB and HB, assuming these have zero intrinsic spread (Fig. 3). Systematic photometric error due to PSF template mismatch in M13 is comparable to that in our earlier cluster studies and simulations judging from the smoothness of the M13 residual images and from the width of its bright RGB (for which the scatter is dominated by systematic error).

The intrinsic shape of the RGB—specifically, the fact that its color gets redder towards the bright end—implies that the brightness ratio between the brightest (bright RGB) stars and faintest (subgiant/turnoff) stars is greater in the I band than in the V band. Detection and photometry of faint stars are affected by the proximity of brighter stars; these crowding effects are somewhat worse in I than in V. Results from the earlier 47 Tuc 1000/F785LP simulation indicate that incompleteness in the matched sample of F555W and F785LP detections sets in about 1 mag brighter than in the sample of 'F555W-only' detections (Fig. 10 of Paper I). Note that M13's bright RGB does not curve over to the red as much as 47 Tuc's since its metallicity is lower than that of 47 Tuc; consequently, the results from the 47 Tuc F785LP simulation may not be applicable to M13 in detail. Figure 2 shows the LFs of the F555W-only sample and the matched F555W and F785LP sample in the central part of M13. The LF of the matched sample turns over due to incompleteness at F555W $\sim$ 18.5, nearly 1 mag brighter than in the F555W-only LF. We return to a discussion of the shape of M13's LF in Sec. 3.5.

3. STELLAR POPULATIONS

3.1. V and I Band Stellar Photometry

The PSF-fitting procedure described in Sec. 2.2 yields a list of positions and F555W brightnesses for 6436 stars in M13 down to $V \sim 21$ within the 1.25 arcmin^2 area of the PC mosaic. The dataset includes stars out to $r < 66''$, but only annuli with $r \lesssim 14''$ are completely contained within the PC image. Of the 6436 F555W detections, 2877 have a corresponding star within $\Delta r < 0\farcs14$ on the F785LP image. This list of 2877 matched F555W and F785LP detections appears to be complete to about $V \sim 18.3$, and hardly any stars with $V > 20$ are detected on the F785LP image (Sec. 2.3, Fig. 2).

The WF/PC-I instrumental calibration constants (Faber 1992) are used to convert the counts (in ADU) reported by the PSF-fitting program into instrumental F555W and F785LP magnitudes. These were then converted to Johnson V and I magnitudes, respectively, using the color transformation equations obtained by Harris et al. (1991). The zeropoints of the F555W and F785LP magnitude systems are roughly equal to those of Johnson V and I, respectively, and there are small but non-zero color terms. Thus, it is only possible to derive magnitudes on the Johnson system for those stars detected in *both* F555W and F785LP.

Figure 3 is a V vs $V - I$ CMD of all stars matched in F555W and F785LP in our M13 sample. The division into different stellar types is only approximate and is based on the gross features of the distribution of stars in the CMD. The data extend below the main sequence turnoff ($V \sim 18.3$, $V - I \sim 0.4$), although they are increasingly incomplete below it. The RGB gets only slightly redder towards its bright end, and the HB droops by almost 3 mag in V and extends quite far to the blue ($V - I \sim -0.5$); these characteristics of M13's CMD are more or less in keeping with its relative low metallicity: [Fe/H] = -1.65 (Djorgovski 1993). A sparse group of asymptotic giant branch (AGB) stars is visible at $V \sim 14$ and $V - I \lesssim 0.8$. A small number of blue straggler stars (BSS) lie in the region slightly brighter and bluer than the main sequence turnoff: $V \lesssim 18$ and $V - I \lesssim 0.4$. The large scatter at the faint end ($V \gtrsim 18.5$) is mostly a result of photometric error.

We have compared the V vs $V-I$ CMD of M13's core (Fig. 3) with ground-based photometry in the B and V bands (Guarnieri et al. 1993; Sandage 1970) and in the B and I bands (Stetson 1996) of stars at a variety of radii in the cluster. While a star-by-star comparison is not possible, a comparison of several fiducial points in the CMD (e.g. RGB color at various levels, HB magnitude and color) indicates that the V and I magnitude zeropoints we have adopted agree with ground-based photometry to within $\sim \pm 0.1$ mag. For the most part however, our study relies on relative photometry of stars and not on absolute photometry.

The positions and brightnesses of a subset of 25 bright ($V \lesssim 13.5$), relatively isolated stars in the core of M13 are listed in Table 1. All positions are on the equinox J2000 coordinate system, and are measured relative to the reference star U (ID#5540) whose coordinates are:

$$\alpha_{\rm J2000}({\rm U}) = 16^{\rm h}41^{\rm m}41\overset{\rm s}{.}61; \quad \delta_{\rm J2000}({\rm U}) = +36^\circ27'42\overset{''}{.}06 \tag{1}$$

The coordinates of star U (accurate to about $0\overset{''}{.}25$) and the position angle of the WF/PC-I images ($38\overset{\circ}{.}46 \pm 0\overset{\circ}{.}5$; see Fig. 1) are based on the *HST* Guide Star Catalog. We adopt Gould & Yanny's (1994) prescription for the pixel scale ($\sim 0\overset{''}{.}044$ pixel^{-1}) and inter-CCD offsets and rotations (Fig. 1) of the PC. The bright stars A–Y listed in Table 1 are marked on the greyscale image of the cluster in Figure 1 and serve as a "finding chart" to facilitate matching our dataset to others. The full version of Table 1 is presented in the AAS CD-ROM Series, volume X, 199X. It contains all 6436 stars detected in the F555W band (with ID#s sorted by right ascension), including the 2877 stars matched in the F555W and F785LP lists for which F555W, F785LP, V, and I magnitudes are provided.

3.2. Blue Stragglers

The V vs $V-I$ CMD of M13 presented in Figure 3 shows a sparse collection of BSS candidates in the region between the main sequence turnoff and the drooping tail of the extended blue HB. About 15 of these BSS candidates lie roughly where the continuation of the upper main sequence would be, if it were to be extrapolated beyond (i.e., brighter and bluer than) the turnoff. These 15 stars are reasonably distinct from the HB and turnoff stars in the CMD and are to be regarded as "likely" candidates. An additional 10 BSS candidates are indicated by the dotted lines in Figure 3. These 10 stars lie close to M13's HB or subgiant branch; some of them may be HB or subgiant stars that have been scattered away from their fiducial locations in the CMD due to measurement error. Thus, these additional 10 BSS are to be considered "possible" candidates. Unless otherwise mentioned, we use the term BSS candidates to refer to all 25 stars.

The actual number of BSSs in the region of M13 covered by our PC image is likely to be in the range 15–25. As discussed in Sec. 2.3, the list of V and I detections should be $> 90\%$ complete down to the main sequence turnoff which makes it unlikely that a BSS would go undetected. Our BSS selection criterion (Fig. 3), while consistent with the criteria used in our earlier studies (Papers I–III) and in previous ground-based studies (cf. Bolte et al. 1993; Stetson 1994), is somewhat arbitrary. In particular, it excludes the less extreme BSSs—those with $V-I$ colors within 0.3 mag and/or V magnitude within 0.5 mag of the turnoff. It is likely that we compensate (possibly overcompensate) for the exclusion of less extreme BSSs from our sample by the including a few "spurious" objects—i.e., turnoff, subgiant, and HB stars that have scattered into the BSS region due to photometric error. A comparative study of 47 Tuc's dense core shows that, of the complete sample of BSSs detected in the ultraviolet study of Paresce et al. (1991), only about half are extreme enough to appear as definite BSSs in a V vs $V-I$ CMD, clearly separated from the turnoff and subgiant branches (Paper I).

The specific frequency of BSS in M13 is calculated according to the definition of Bolte et al. (1993): $F_{\rm BSS} = N({\rm BSS})/N(V < V_{\rm HB} + 2)$. Although M13's HB is not truly horizontal in the CMD (Fig. 3), it has a well defined brightness of $V \approx 15$ at the location of the RR Lyrae instability region before drooping to fainter V magnitudes at the blue end. There are 343 subgiants in the M13 PC image that fulfil the criterion for the normalizing population. The specific frequency is $F_{\rm BSS} = 0.04$ if we count only the 15 definite BSS candidates in M13's core, and $F_{\rm BSS} = 0.07$ if we count all 25 candidates. The 1σ Poisson error in the specific frequency is $\delta F_{\rm BSS} = 0.01$, but systematic errors in the BSS sample selection are likely to be somewhat larger.

Table 2 compares M13's BSS frequency to that of a few other globular clusters (listed in order of decreasing stellar density) that have been studied recently. As pointed out by Sosin & King (1995), it is interesting that the BSS frequency in this representative set of clusters spans only a range of a factor of three, with a mean value of $F_{\rm BSS} \sim 0.11$, despite the $\gtrsim 10^4$ range in stellar density among the clusters. M13's BSS frequency is also within this relatively narrow range.

3.3. Radial Distribution of Stellar Populations

In this section, we compare the radial density distributions of the various types of evolved stars found in M13's core. The cluster core fills most of the field of view of the PC mosaic, so our sample spans only a small range of stellar space densities (roughly a factor of 8). We divide the sample of stars into four (projected) radial bins: (1) $r < 15\farcs0$, (2) $15\farcs0 \leq r < 25\farcs8$, (3) $25\farcs8 \leq r < 37\farcs6$, and (4) $37\farcs6 \leq r < 65\farcs6$, around the cluster center. We define the cluster center to be the centroid of the light distribution as measured on a ground-based image of M13:

$$\alpha_{\rm J2000}(0) = 16^{\rm h}41^{\rm m}41\fs2; \quad \delta_{\rm J2000}(0) = +36^{\circ}27'35'' \tag{2}$$

These coordinates are within $4''$ of the cluster centroid coordinates quoted by Djorgovski (1993), well within the measurement errors. The limiting radii of the four radial bins have been chosen so that each bin contains the same number of stars with $V < 18$. This relatively bright subsample of stars, dominated in number by subgiants and faint RGB stars, is complete at all radii (Sec. 2.3) and serves as a convenient normalizing population in studying the radial distribution of various stellar types. The first three radial bins are entirely within the core of M13 ($r_{\rm core} = 38''$). The rectangular field of view of the PC includes only a fraction of the annulus for bins 2, 3, and 4 (56%, 42%, and 18%, respectively).

Figure 4 is a composite of the CMDs in each of the four radial bins. There are no striking differences in the mix of stellar types between annuli. The innermost bin appears to be somewhat deficient in HB stars (quantified below). The turnoff portion of the CMD has slightly less scatter and a higher number of stars as one moves radially outwards, a result of improved photometric accuracy and increased degree of completeness in the sparser parts of the cluster.

Table 3 lists the number of stars of each type in the four radial bins. The division of the post main sequence stars in M13 into various stellar types is defined by the dashed lines in Figure 3. The total number of stars increases towards larger radii due to the increased probability of detecting faint turnoff stars and main sequence stars ($V \sim 20$). Faint RGB stars and subgiants make up the bulk of the normalizing population used to define the limiting radii, so it is not surprising that their numbers are roughly constant across the four bins. There is no radial gradient in the fraction of bright RGB or BSS stars either. Poisson errors are very large for the BSS population; small changes in the BSS fraction as a function of radius (smaller than a factor of 2–3) would be undetectable in our sample of 25 candidates. The HB stars show a marginal central depletion. Their expected number per bin is 21 ± 4.6 (1σ). The HB population of the innermost radial bin appears to be about 55% of the expected number, and is low by -1.7σ.

The cumulative radial distributions of different types of stars in the core of M13 are plotted in Figure 5. A two-sided Kolmogorov–Smirnov test shows that the radial distributions of the faint RGB/subgiant, bright RGB/AGB, and BSS populations are consistent with one another. The HB stars show a marginal central depletion relative to the faint RGB/subgiant stars (82% significance level or $\sim 1.5\sigma$). The radial distribution of faint RGB/subgiant stars in M13 is well fit by a King profile (King 1962) of core radius $r_{\rm core} = 38''$ (1.3 pc) as indicated by the thin solid curve in Figure 5. The 90% confidence limit on the core radius of M13's RGB stars is $\pm 6''$. The HB stars, on the other hand, have a core radius of $r_{\rm core,\, HB} \gtrsim 60''$. It is perhaps not surprising that Trager et al. (1993) found a best fit core radius of $r_{\rm core} = 53''$ for the overall surface brightness distribution (intermediate between the RGB and HB core radii), since RGB stars and HB stars together account for most of the visual light in M13.

3.4. Radial Population Gradients in Three King Model Clusters: M13, M3, and 47 Tuc

Subtle (but real) radial gradients in the stellar populations of globular clusters may be masked by large statistical errors in the measurement of the stellar density that result from having a limited number of stars in the core of a single cluster. To reduce the Poisson errors associated with the measurement of population gradients, we combine samples of post main sequence stars from five dense clusters: M13, M3, 47 Tuc, M30, and M15. The cumulative distributions of the subsamples of faint RGB/subgiant and HB stars in this combined sample are plotted as a function of the projected $r/r_{\rm half\ light}$ in the upper panel of Figure 6. The lower panel of Figure 6 shows the cumulative radial distribution vs $r/r_{\rm core}$ for the combined faint RGB/subgiant and HB samples from the three King model clusters only: M13, M3, and 47 Tuc.

The following values of $r_{\rm half\ light}$ ($r_{\rm core}$) have been adopted: $93''$ ($38''$, Sec. 3.3) for M13, $68''$ ($28''$, Paper III) for M3, $174''$ ($23''$, Paper I) for 47 Tuc, $62''$ for M30, and $60''$ for M15. Half light radii are taken from Trager et al. (1993); M30 and M15 do not have well defined core radii. The data extend out to $66''$ ($0.7\, r_{\rm half\ light}$, $1.7\, r_{\rm core}$) in M13, $65''$ or $1.0\, r_{\rm half\ light}$ ($2.3\, r_{\rm core}$) in M3, $61''$ or $0.4\, r_{\rm half\ light}$($2.7\, r_{\rm core}$) in 47 Tuc, $130''$ or $2.1\, r_{\rm half\ light}$ in M30, and $130''$ or $2.2\, r_{\rm half\ light}$ in M15.

There are 2648 faint RGB/subgiant stars in the five-cluster sample (248 from M13, 375 from M3, 561 from 47 Tuc, 290 from M30, and 1174 from M15) and 1184 in the three-cluster sample; the distribution of faint RGB/subgiant stars among the clusters indicates the relative weight given to each cluster in the combined cumulative distribution. Note that the data for the five clusters extend out to different values of $r/r_{\rm half\ light}$ and $r/r_{\rm core}$. Thus, it is necessary to ensure that the ratio of faint RGB/subgiant to HB (or BSS) stars is the same for each cluster to avoid radially biasing the population ratio. We adjust the size of the faint RGB/subgiant sample in each cluster (by changing the faint end limiting magnitude) so that the ratio of HB (or BSS) to faint RGB/subgiant stars is the same in each cluster.

Two-sided Kolmogorov–Smirnov tests were performed on the cumulative radial distribution functions of the combined three- and five-cluster samples for the BSS vs faint RGB/subgiant and HB vs faint RGB/subgiant stellar populations. The BSSs are marginally centrally concentrated relative to the normalizing population (85% confidence level) in the three-cluster sample. The central concentration of BSSs in the combined three-cluster sample is of comparable significance to that in M3 (86% confidence—Paper III) and is *less* significant than in 47 Tuc (90%–95% confidence—Paper I); the nature of the BSS concentration is sufficiently different in M3 and 47 Tuc that the effect is not reinforced in the combined sample. In the five-cluster sample, the BSSs are significantly more centrally concentrated than the normalizing faint RGB/subgiant population: the probability that the two populations are drawn from the same radial distribution is only 10^{-5}; this is largely driven by the numerous, strongly centrally concentrated BSSs in M30.

The HB stars in the combined sample show some evidence for central depletion relative to the faint RGB/subgiant stars. The depletion is significant at the 85% confidence level in the three-cluster sample ($\sim 1.5\sigma$), and at the 97% level in the five cluster-sample ($\sim 2\sigma$). Is interesting to note that each of the the five dense globular clusters that we have studied in our *HST* program so far displays a weak (and only marginally significant in each individual cluster) central HB deficiency: M13 (Fig. 6), M3 (Fig. 12 of Paper III; Bolte et al. 1993), 47 Tuc (Fig. 18 of Paper I), M30 (Fig. 5 of Yanny et al. 1994b), and M15 (Fig. 18 of Paper II). As noted by Laget et al. (1992), studies of M14, M15, and NGC 6397 suggest that red HB stars (those redder than the RR Lyrae gap) may be more centrally concentrated than blue HB stars; our samples indicate no obvious difference between the degree of depletion of red HB stars (47 Tuc) and blue HB stars (M30, M13) in cluster cores. Furthermore, a WFPC2 study of M15 shows that the red and blue HB stars in this cluster have similar radial density distributions (Guhathakurta et al. 1996).

The cause of the central HB depletion in dense globular cluster cores remains a mystery. It is unlikely to be due to mass segregation between HB stars and the more massive subgiants because: (1) the dynamical time scale for mass segregation in the cores of these dense clusters, $t_{\rm dyn} \approx 10^9$ yr (Djorgovski 1993), is larger than the time spent by a star in the HB phase, $t_{\rm HB} \approx 10^8$ yr (Lee & Demarque 1990); and (2) standard stellar evolution theory (Lee et al. 1990) predicts only a small amount of mass loss in the RGB phase and hence only a small difference in mass between an HB star ($\gtrsim 0.7\,M_\odot$) and a subgiant ($0.8\,M_\odot$).

The central HB depletion is not an artifact of a higher rate of misidentification of HB stars near the cluster center than in the outer parts. Firstly, for relatively bright stars such as HB stars, the photometric errors are fairly small ($1\sigma \sim 0.1$ mag) and do not vary appreciably with distance from the cluster center (especially in the case of M13 where the stellar density does not vary drastically over the area of the PC image). Secondly, the section used to define HB stars in the CMD (cf. Fig. 3) is large enough that HB stars are unlikely to scatter out of the region because of photometric error.

3.5. Luminosity Function

Figure 7 shows the LF of evolved stars in the PC image of M13 (open bold symbols). The LF is plotted versus stellar F555W magnitude, and not the transformed Johnson V magnitude which requires both F555W and F785LP measurements. As discussed in Sec. 2.3, the sample of F555W-only detections from which the LF is derived is more complete at the faint end than the sample of "matched" F555W and F785LP detections. Incompleteness sets in fainter than F555W ~ 19 in the F555W-only sample; at brighter magnitudes, the LF shape appears to be independent of radial distance from the center of M13 (Fig. 2). We therefore combine data from the entire PC image to minimize Poisson error (1σ error bars are shown in Fig. 7). Even though detection in the F555W band is the only criterion used to select stars for the LF, in practice, the brightest stars are detected in both F555W and F785LP bands. For reasons explained below, we use a color cut ($V - I < 0.4$) to exclude HB stars and to restrict the bright part of the LF (F555W < 17.3) to only RGB and AGB stars.

The dashed line in Figure 7 shows a theoretical model for the LF of an old (16 Gyr), metal-poor ([Fe/H] $= -1.66$) stellar population (Bergbusch & Vandenberg 1992). These parameters have been chosen to match the age (14.6 ± 3.0 Gyr—Carney et al. 1992) and metallicity ([Fe/H] $= -1.65$—Djorgovski 1993) of M13. The absolute visual magnitude scale in the model LF has been converted to the apparent F555W magnitude scale using a distance modulus of $(m - M)_0 = 14.29$ mag and a Galactic extinction of $A_V = 0.06$ mag for M13 (Djorgovski 1993). The model LF has been normalized to match the observed number stars at F555W = 19, (conservatively) assuming that the M13 sample is only 90% complete for stars of this apparent brightness (see Sec. 2.3). The Bergbusch–Vandenberg model does not include the HB phase of stellar evolution; hence we have excluded HB stars from M13's LF before comparing it to the model LF. Fainter than F555W = 19, the observed LF falls below the model LF due to the effect of incompleteness, as predicted by our image simulations.

A comparison between M13's LF and the Bergbusch–Vandenberg model LF (Fig. 7) shows that the model underpredicts the number of bright RGB stars relative to the subgiants. Specifically, there are twice as many bright RGB stars in the range $V = 12.5$–15 in M13 than predicted by the model, a 6.4σ difference (taking only Poisson error into account). Note, the M13 LF includes both RGB and AGB stars at its bright end (since the PC photometry is not accurate enough to allow a clear distinction between these two classes) whereas the Bergbusch–Vandenberg model LF includes only RGB stars. In order to resolve the difference between the model and data, roughly half the bright stars in M13 ($V \lesssim 15$) would have to be AGB stars. This seems unlikely since AGB stars typically make up a small fraction of the bright end of the LF in globular clusters: $N(\mathrm{AGB})/N(\text{bright RGB}) \approx N(\mathrm{AGB})/N(\mathrm{HB}) \approx 0.15$ (Renzini & Fusi Pecci 1988; Buzzoni et al. 1983; Buonanno et al. 1985). Furthermore, we have obtained a ground-based CMD of stars in M13 with sufficient photometric accuracy to distinguish AGB stars from bright RGB stars, and this indicates a comparably small AGB fraction at the bright end of M13's LF.

The discrepancy in the number of bright RGB stars between M13 and the model is not a result of incorrect normalization of the model; the model is in excellent agreement with the data for the faint RGB, subgiant, and turnoff stars (F555W = 15–18.5). The horizontal offset of the model LF (along the F555W magnitude scale), derived from the quoted M13 distance modulus and line-of-sight visual extinction, is also in good agreement with the data judging from the sharp upturn in both LFs at the base of the giant branch at F555W ≈ 17. Moreover, varying the metallicity of the model over the range, $-2 \lesssim [\mathrm{Fe/H}] \lesssim -1$, and its age over the range, 8 Gyr $< t <$ 18 Gyr, does not make a significant difference to the quality of the fit.

Discrepancies between the relative numbers of RGB stars and turnoff stars have also been noted in the clusters M92 (Stetson 1991) and M30 (Bolte 1994). Unlike the case of M13, where there is only a discrepancy for the brightest RGB stars, these other two clusters display an excess of faint as well as bright RGB stars relative to turnoff stars. Larson et al. (1995) suggest that a modification of the canonical stellar model to include the effects of internal rotation might boost the lifetimes of faint RGB stars and subgiants enough to resolve the discrepancy for such stars; their models, however, do not examine the effects of rotation in bright RGB stars (those at or above the HB level) and therefore do not address the problem of M13's LF directly. Interestingly, a recent study of M5 shows good agreement between the observed LF and that predicted by the canonical Bergbusch–Vandenberg model (Sandquist et al. 1996). A systematic study of the LFs of evolved stars in globular clusters is needed to determine what fraction of clusters display this RGB excess and what global property of the cluster might be correlated with the excess. A thorough investigation of model parameter space is currently in progress (Vandenberg 1996, private communication). For now, the question of what causes the RGB discrepancy remains unanswered.

4. SUMMARY

The principal results obtained in this paper are summarized below:

1. *Hubble Space Telescope* (pre-refurbishment) Planetary Camera-I images in the F555W (V) and F785LP (I) bands of the central $68'' \times 68''$ region of the dense globular cluster M13 (NGC 6205) have been analyzed. A table is presented containing relative astrometry and photometry in the F555W, F785LP, V, and I bands of 2877 post main sequence stars within $r < 66''$ of the cluster center, and F555W photometry of an additional 3559 faint stars ($V \approx 18$–21).

2. Fifteen blue straggler candidates and 10 other possible BSS candidates are identified in the core of M13 on the basis of a V vs $V - I$ color–magnitude diagram. The specific frequency of BSS in M13, $F_{\rm BSS} \equiv N({\rm BSS})/N(V < V_{\rm HB} + 2) = 0.04$–$0.07$, is comparable to the value measured in other dense clusters. The radial distribution of BSSs is consistent, within Poisson error, with that of other stellar types.

3. The radial surface density profiles of the bright red giants, faint red giants, subgiants, and turnoff stars are consistent with one another. These stars are well fit by a King profile of core radius $r_{\rm core} = 38'' \pm 6''$ (1.3 pc). Horizontal branch stars appear to be centrally depleted relative to the giants and subgiants (only a $\gtrsim 1.5\sigma$ effect), and their distribution is better described by an $r_{\rm core,\, HB} \gtrsim 60''$ King profile.

4. There is a hint of a slight central HB deficiency in each of the five dense globular clusters we have studied to date: M13, M3, 47 Tuc, M30, and M15; the significance of this effect in each cluster, however, is marginal. Samples of various stellar types from these clusters are combined to derive the cumulative radial distribution as a function of $r/_{\rm half\ light}$; the three King model clusters, M13, M3 and 47 Tuc are combined in

terms of $r/_{\rm core}$. The HB stars appear to be less centrally concentrated than the giants (97% and 85% significance in the five- and three-cluster samples, respectively). The BSS stars in the combined five-cluster sample are more centrally concentrated than the giants ($> 5\sigma$ effect).

5. The stellar luminosity function of M13 in the F555W (V) band is compared to a suitably normalized, standard model LF for an old, metal-poor population (Bergbusch & Vandenberg 1992). The model is a good match to the shape of the observed LF for stars in the brightness range $V \sim 15$–19 (the M13 sample is incomplete at fainter magnitudes). However, the relative number of bright red giants in M13 ($V \lesssim 15$) is a factor of two higher than predicted by the model.

We would like to thank John Faulkner, Eric Sandquist, and Dennis Zaritsky for useful discussions and the referee, George Djorgovski, for helpful tips on combining cluster samples. We are grateful to Zodiac Webster for allowing us to include unpublished work on M30 in Sec. 3.4. P.G. would like to thank the Institute for Advanced Study for its generous hospitality. This research was supported in part by NASA through Grant No. NAG5-1618 and Grant No. HF-1033.01-93B from the Space Telescope Science Institute, which is operated by the Association of Universities for Research in Astronomy, Inc., under NASA Contract No. NAS5-26555.

APPENDIX: TABLE OF STARS

The full version of Table 1 contains photometry in the F555W band (similar, but not identical, to V) and relative astrometry for 6436 evolved stars down to $V \sim 21$ in M13's core region. In addition, F785LP, V, and I photometry is presented for 2877 of these stars.

A subset of Table 1, containing the 25 brightest stars in the core of M13, appears in this paper; the full version is published in the AAS CD-ROM Series, volume X, 199X. Computer-readable copies of the full table may be obtained via anonymous ftp as follows:

- `ftp eku.sns.ias.edu` (login as: `anonymous`)
- `cd pub/GLOBULAR_CLUSTERS/m13`
- `get tbl.cdrom`

or by contacting P.G. or R.L.C..

Details of the photometric procedure and estimates of the completeness and photometric accuracy may be found in Sec. 2 and references therein. The reader is referred to Sec. 3.1 for a brief description of the astrometric convention and the parameters used in astrometric solution (see also Fig. 1). We recommend that the astrometry provided in Table 1 be matched empirically against other datasets, to correct for possible systematic errors in the scale, translation, and rotation of the coordinate system we have adopted.

References

Baum, W. A., Hiltner, W. A., Johnson, H. L., & Sandage, A. R. 1959, ApJ, 130, 749

Bergbusch, P. A., & Vandenberg, D. A. 1992, ApJS, 81, 163

Bolte, M. 1994, ApJ, 431, 223

Bolte, M., Hesser, J. E., & Stetson, P. B. 1993, ApJ, 408, L89

Buonanno, R., Corsi, C. E., & Fusi Pecci, F. 1985, A&A, 145, 97

Burrows, C. J., Holtzman, J. A., Faber, S. M., Bely, P. Y., Hasan, H., Lynds, C. R., & Schroeder, D. 1991, ApJ, 369, L21

Buzzoni, A., Fusi Pecci, F., Buonanno, R., & Corsi, C. E. 1983, A&A, 123, 94

Carney, B. W., Storm, J., & Jones, R. V. 1992, ApJ, 386, 663

Cudworth, K. M., & Monet, D. G. 1979, AJ, 84, 774

Djorgovski, S. G. 1993, in Structure and Dynamics of Globular Clusters, edited by S. G. Djorgovski and G. Meylan (ASP Conf. Series, No. 50), p. 373

Faber, S. M. (editor) 1992, Final Orbital/Science Verification Report, Space Telescope Science Institute Pulication

Gould, A., & Yanny, B. 1994, PASP, 106, 101

Griffiths, R. 1989, Wide Field and Planetary Camera Instrument Handbook, Space Telescope Science Institute Pulication

Guarnieri, M. D., Bragaglia, A., & Fusi Pecci, F. 1993, A&AS, 102, 397

Guhathakurta, P., Yanny, B., Bahcall, J. N., & Schneider, D. P. 1994, AJ, 108, 1786 (Paper III)

Guhathakurta, P., Yanny, B., Schneider, D. P., & Bahcall, J. N. 1992, AJ, 104, 1790 (Paper I)

Guhathakurta, P., Yanny, B., Schneider, D. P., & Bahcall, J. N. 1996, AJ (in preparation)

Harris, H. C., Baum, W. A., Hunter, D. A., & Kreidl, T. J. 1991, AJ, 101, 677

King, I. R. 1962, AJ, 67, 471

Laget, M., Burgarella, D., Milliard, B., & Donas, J. 1992, A&A, 259, 510

Larson, A. M., Vandenberg, D. A., & Depropris, R. 1995, BAAS, 27, 1431

Lauer, T. R. 1989, PASP, 101, 445

Lee, Y.-W., & Demarque, P. 1990, ApJS, 73, 709

Lee, Y.-W., Demarque, P., & Zinn, R. 1990, ApJ, 350, 155

Lupton, R. H., & Gunn, J. E. 1986, 91, 317

Lupton, R. H., Gunn, J. E., & Griffin, R. F. 1987, AJ, 93, 1114

Nemec, J. M., & Cohen, J. G. 1989, ApJ, 336, 780

Paez, E., Straniero, O., & Martinez Roger, C. 1990, A&AS, 84, 481

Paresce, F., et al. 1991, Nature, 352, 297

Pryor, C., & Meylan, G. 1993, in Structure and Dynamics of Globular Clusters, edited by S. G. Djorgovski and G. Meylan (ASP Conf. Series, No. 50), p. 357

Renzini, A., & Fusi Pecci, F. 1988, ARA&A, 26, 199

Sandage, A. R. 1970, ApJ, 162, 841

Sandquist, E. L. 1996, private communication

Sandquist, E. L., Bolte, M., & Stetson, P. B. 1996, ApJ (in press)

Savedoff, M. P. 1956, AJ, 61, 254

Sosin, C., & King, I. R. 1995, AJ, 109, 639

Stetson, P. B. 1987, PASP, 99, 191

Stetson, P. B. 1991, in Formation and Evolution of Star Clusters, edited by K. Janes (ASP Conf. Series, No. 13), p. 88

Stetson, P. B. 1992, in Astronomical Data Analysis Software, edited by D. M. Worrall, C. Biemesderfer, and J. Barnes (ASP Conf. Series, No. 25), p. 297

Stetson, P. B. 1994, PASP, 106, 250

Stetson, P. B. 1996, preprint

Trager, S. C., Djorgovski, S., & King, I. R. 1993, in Structure and Dynamics of Globular Clusters, edited by S. G. Djorgovski and G. Meylan (ASP Conf. Series, No. 50), p. 347

Yanny, B., Guhathakurta, P., Bahcall, J. N., & Schneider, D. P. 1994a, AJ, 107, 1745 (Paper II)

Yanny, B., Guhathakurta, P., Schneider, D. P., & Bahcall, J. N. 1994b, ApJ, 435, L39

Zinn 1986, in Stellar Populations, edited by C. Norman, A. Renzini, and M. Tosi (Cambridge University Press), p. 73

Table 1.
Selected Bright Stars in the Core of M13

ID#[a]	ID[b]	Offset in [″] from U		CCD	r	Instr. mags.		Johnson mags.		
		$\Delta\alpha_{\rm J2000}$	$\Delta\delta_{\rm J2000}$	[PC#]	[″]	F555W	F785LP	V	I	$V-I$
2289	A	−28.84	−18.55	7	26.9	12.20	10.66	12.14	10.81	1.33
3772	B	−15.98	−9.60	6	11.7	12.22	10.79	12.17	10.94	1.23
1103	C	−41.61	8.22	5	40.0	12.57	11.35	12.52	11.47	1.05
2851	D	−23.58	−3.02	5	19.4	12.65	11.25	12.60	11.39	1.21
6428	E	17.70	−5.21	6	22.4	12.66	11.58	12.61	11.68	0.93
5610	F	0.92	−22.33	6	16.3	12.67	11.54	12.62	11.65	0.97
758	G	−46.77	14.67	5	47.4	12.69	11.34	12.63	11.47	1.16
4982	H	−5.95	−18.11	6	11.2	12.70	11.47	12.65	11.59	1.06
1203	I	−40.26	−4.32	8	35.8	12.74	11.49	12.69	11.61	1.08
4976	J	−5.99	13.09	6	20.1	12.74	11.55	12.69	11.66	1.03
5407	K	−1.58	9.72	6	17.0	12.77	11.45	12.72	11.58	1.14
2739	L	−24.59	−19.86	7	23.8	12.95	11.73	12.90	11.85	1.05
2107	M	−30.87	−16.68	7	28.0	12.98	11.71	12.93	11.84	1.09
1439	N	−37.57	−24.52	7	37.4	13.04	11.75	12.99	11.88	1.11
2581	O	−26.00	−31.50	7	32.5	13.15	12.03	13.10	12.13	0.97
6275	P	10.68	−10.90	6	15.8	13.21	12.01	13.16	12.13	1.03
2878	Q	−23.36	−10.09	7	19.0	13.22	12.10	13.17	12.20	0.97
3076	R	−21.67	−46.30	7	42.9	13.22	12.09	13.17	12.20	0.97
4204	S	−12.45	5.10	6	14.4	13.21	12.26	13.17	12.35	0.82
2204	T	−29.76	6.25	5	28.5	13.31	12.20	13.27	12.31	0.96
5540	U	0.00	0.00	6	8.4	13.41	12.08	13.35	12.20	1.15
1118	V	−41.38	−17.90	8	38.4	13.47	12.39	13.42	12.49	0.93
4841	W	−7.19	−6.16	6	2.7	13.48	12.41	13.43	12.51	0.92
673	X	−48.09	−24.79	8	47.0	13.52	12.58	13.47	12.66	0.81
4009	Y	−14.22	−41.45	7	35.8	13.60	12.47	13.56	12.59	0.97

[a] ID#s from the complete version of Table 1 which is sorted by right ascension (see text).

[b] Letter IDs are sorted by V brightness and are shown in Figure 1.

TABLE 2.
A Comparison of Blue Straggler Frequencies

Cluster	$F_{\rm BSS}$	Region Studied[a]	[pc]	ρ_0^a $[M_\odot\,{\rm pc}^{-3}]$	Source
M13	0.04–0.07	$r \lesssim 1.7\,r_{\rm core}$	2.3	2.5×10^3	This paper
M15	0.06 ± 0.01	$r \lesssim 15\,r_{\rm core}^b$	1.7	1.6×10^6	Guhathakurta et al. (1996)
M30	0.19 ± 0.04	$r \lesssim 10\,r_{\rm core}^b$	0.7	8×10^5	Yanny et al. (1994b)
47 Tuc	0.07 ± 0.01^c	$r \lesssim 3\,r_{\rm core}$	1.6	1.3×10^5	Paper I
M3	0.09 ± 0.02^d	$r \lesssim 0.7\,r_{\rm core}$	1.0	3.2×10^3	Paper III
NGC 5053	0.14 ± 0.03	$r < 1\,r_{\rm core}$	10	4	Nemec & Cohen (1989)
M3[e]	0.09 ± 0.03	$r \sim 15\,r_{\rm core}$	20	1^e	Paez et al. (1990)

[a] Central density and distance: Pryor & Meylan (1993); core radius: Djorgovski (1993).

[b] The core radius is poorly defined for the post core collapse clusters M15 and M30; we arbitrarily assume $r_{\rm core} = 2''$, the rough upper limit to their core radii.

[c] Corrected for the 50% BSS detection efficiency in our V- and I-band WF/PC-I data.

[d] Bolte et al.'s (1993) ground-based study of the core of M3 found a BSS frequency of only 0.04, but their data were shown to be incomplete (Paper III).

[e] The space density of stars in this outer M3 field is expected to be about 3×10^{-4} of the central value.

TABLE 3.
Radial Distribution of Evolved Stellar Populations in M13

	Limiting Radii			
Stellar Subsample	$r<15''.0$	$15''.0 \le r < 25''.8$	$25''.8 \le r < 37''.6$	$37''.6 \le r < 65''.6$
Bright stars ($V < 18.0$)[a]	233	235	234	234
All stars ($V \lesssim 20$)	643	668	731	835
Faint RGB/subgiants	180	180	169	176
Bright RGB/AGB	32	29	34	27
HB	13	22	24	25
BSS (all candidates)	8	4	7	6

[a] The sample should be complete to this limiting magnitude; the limiting radii were chosen to include the same number of bright stars in each radial bin.

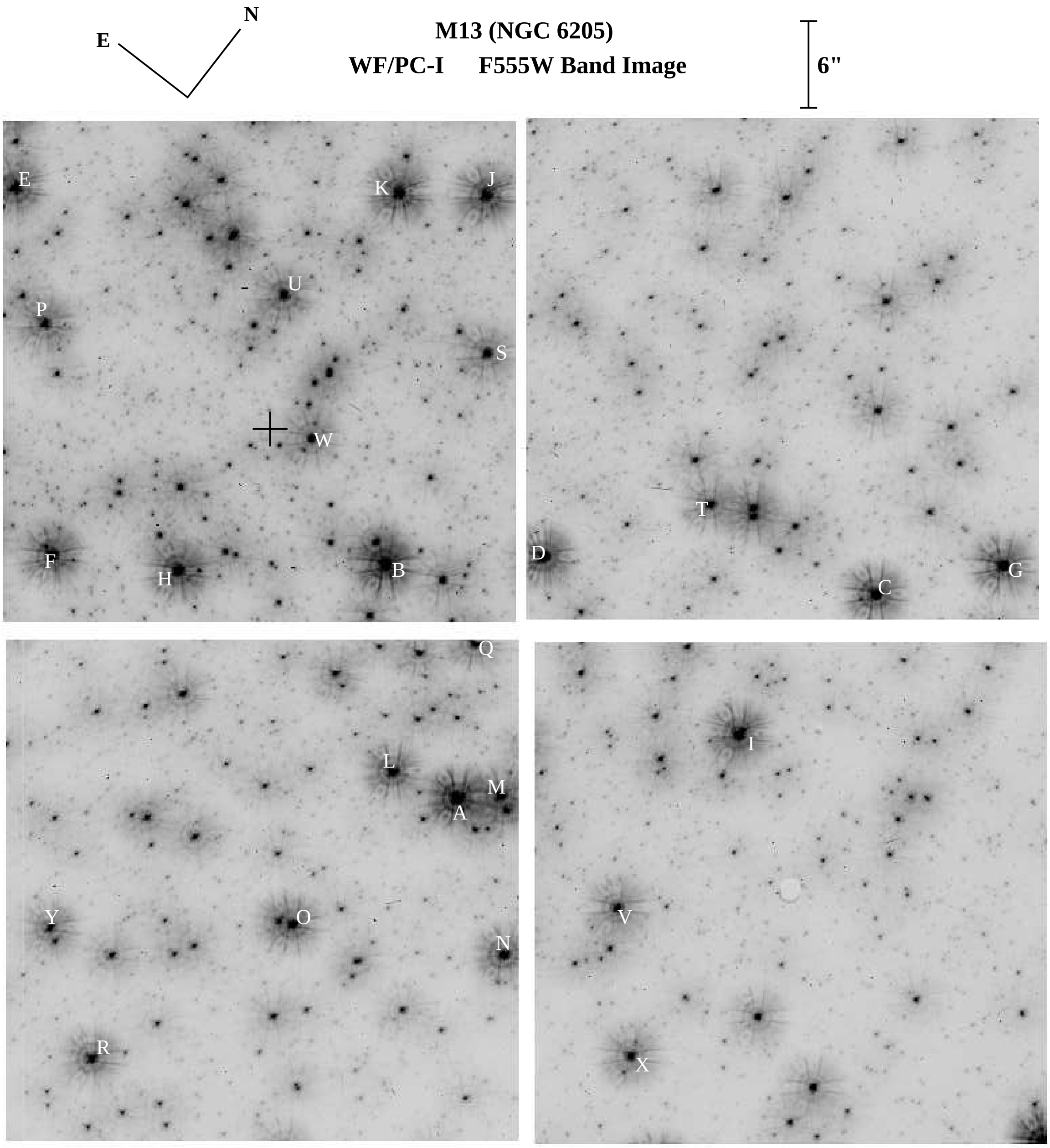

Fig. 1.— A negative (color-reversed) *HST* F555W image of the core of M13. The PC mosaic consists of CCDs PC5–PC8, with PC5 in the upper right and continuing counterclockwise. The gaps between the four CCD frames are represented approximately to scale. A selected set of bright, relatively isolated reference stars are identified by the letters A–Y; the positions and brightnesses of these reference stars are listed in Table 1. The "+" near the center of PC6 marks the cluster centroid and the density of stars is highest on PC6. The scale and orientation of the image are indicated (vertical is 38°.46 East of North).

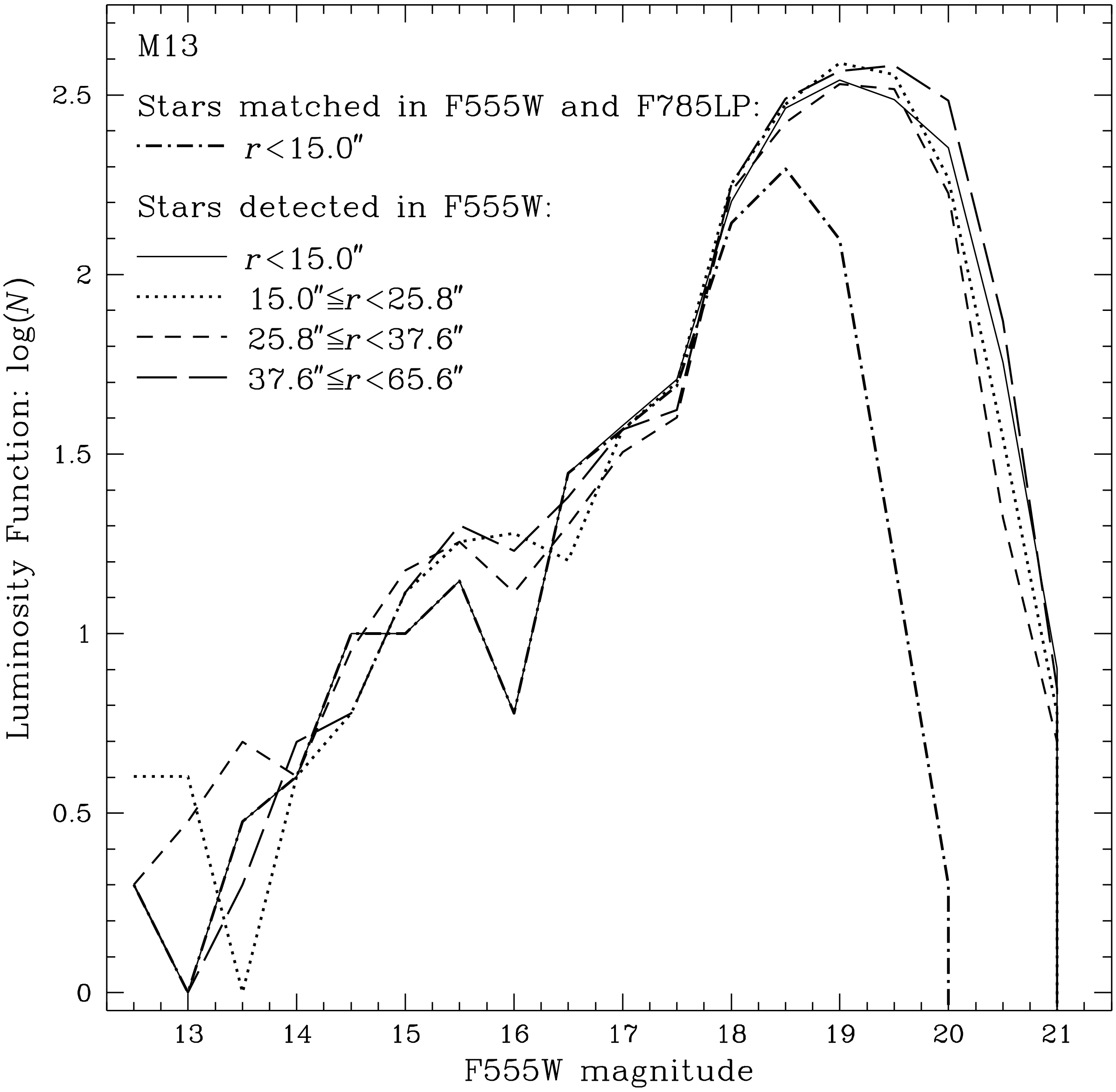

Fig. 2.— The observed stellar luminosity function of M13 in the F555W band (roughly similar to Johnson V) in four concentric radial bins. The rollover beyond F555W $\sim$ 19 is caused by incompleteness. The bold dot-dashed line represents stars in the innermost radial bin that are detected in both F555W and F785LP bands; incompleteness sets in about 1 mag brighter in this sample than in the corresponding F555W-only sample. The weak bump at F555W $\sim$ 15–16 is caused by stars in the extended blue HB.

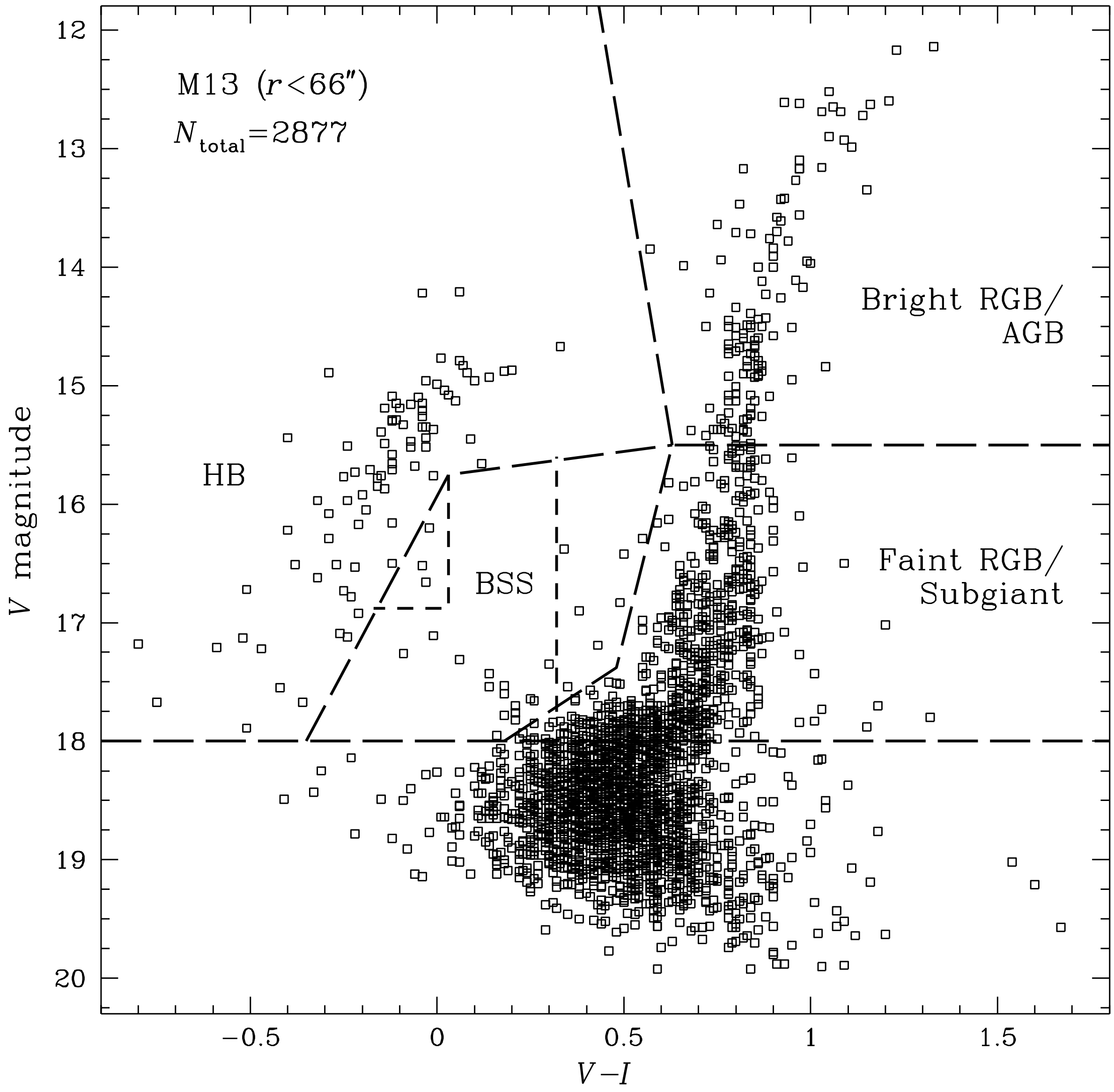

Fig. 3.— A color–magnitude diagram of all 2877 matched F555W and F785LP detections in M13 ($r < 66''$). The dashed lines indicate the boundaries that have been used to distinguish between various stellar types. The dotted lines in the blue straggler star (BSS) region enclose the 10 "possible" BSS candidates. The sample is increasingly incomplete fainter than $V \sim 18.5$, below the main sequence turnoff.

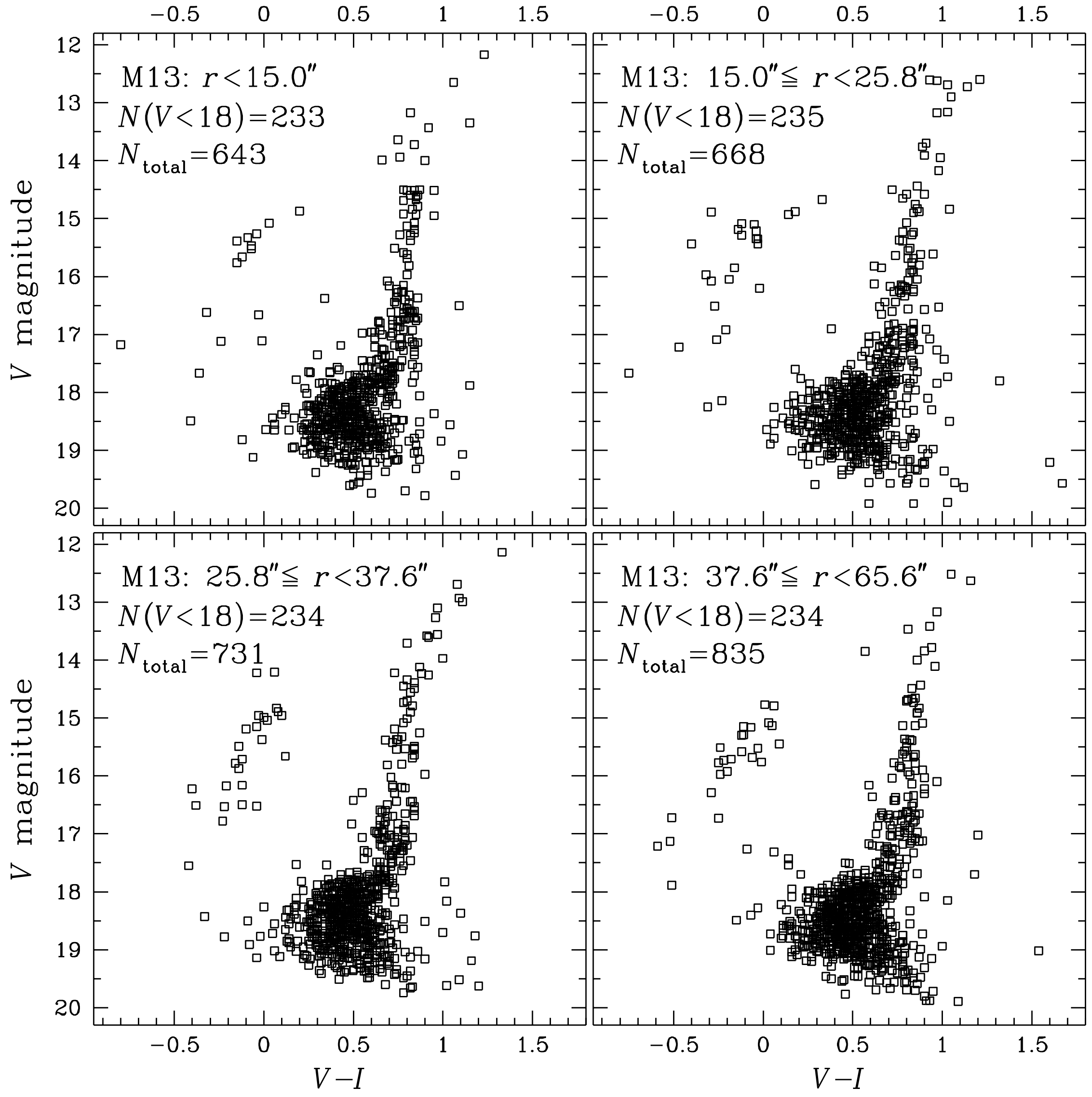

Fig. 4.— A composite of V vs $V-I$ color–magnitude diagrams in four radial bins around the approximate center of M13. The limiting radii have been chosen to ensure that the bins contain equal numbers of stars with $V<18$ (the sample is complete down to this limiting magnitude). The degree of completeness for faint ($V \gtrsim 18$), turnoff stars is somewhat higher in the outer bins (3 & 4) than in the inner bins. The radial bins do *not* represent entire annuli. The innermost bin appears to be slightly deficient in horizontal branch stars relative to the bins further out.

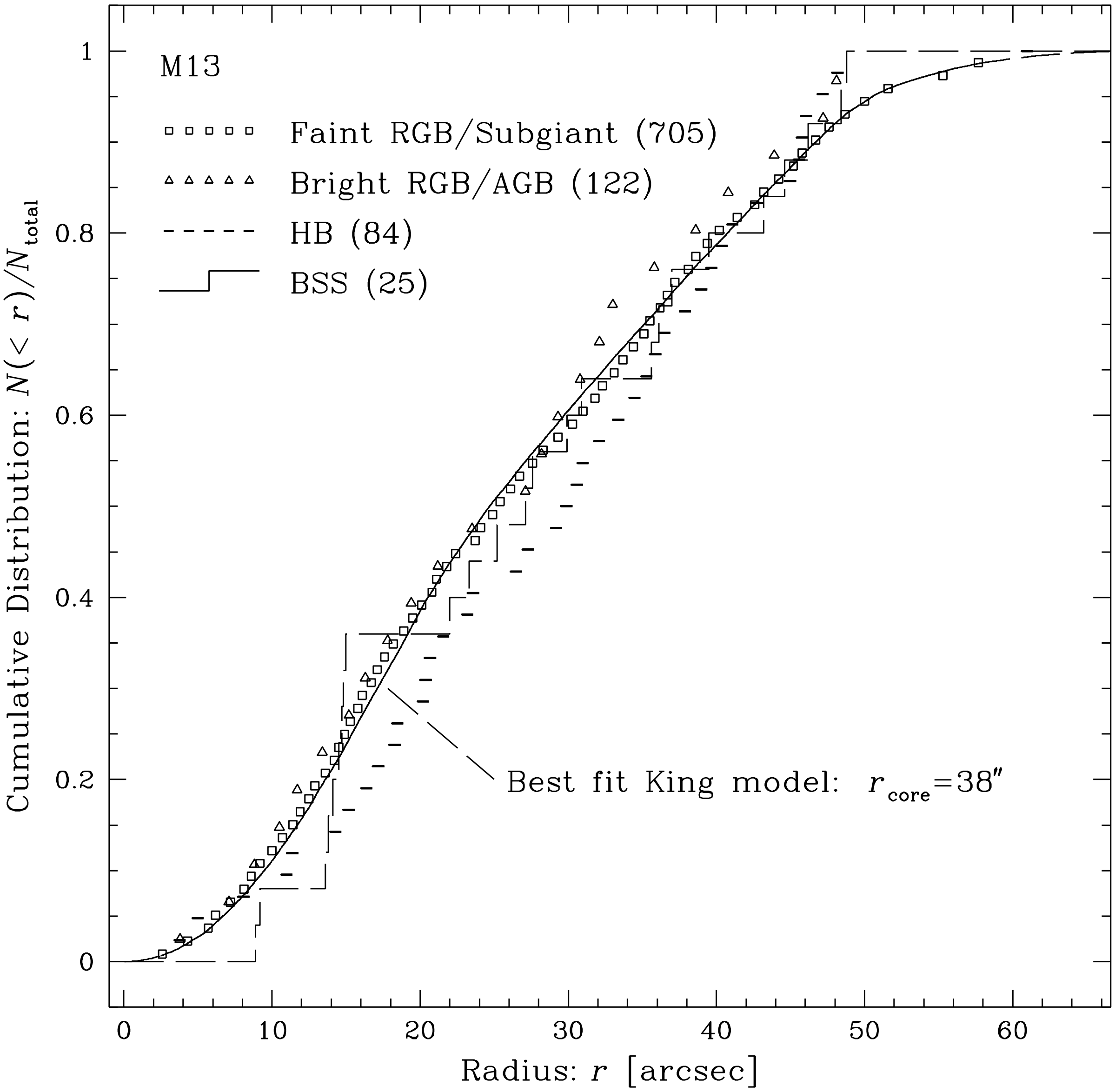

Fig. 5.— The cumulative radial distribution of different kinds of post main sequence stars in M13. Only every second HB star, every fifth bright RGB/AGB star, and every tenth faint RGB/subgiant star is shown for the sake of clarity. The smooth solid line shows an $r_{\rm core} = 38''$ King profile; this is consistent with the radial distribution red giants to within Poisson errors. The numbers within parentheses indicate the number of stars of each type. There is a suggestion that the HB stars have a weaker degree of central concentration than the giants.

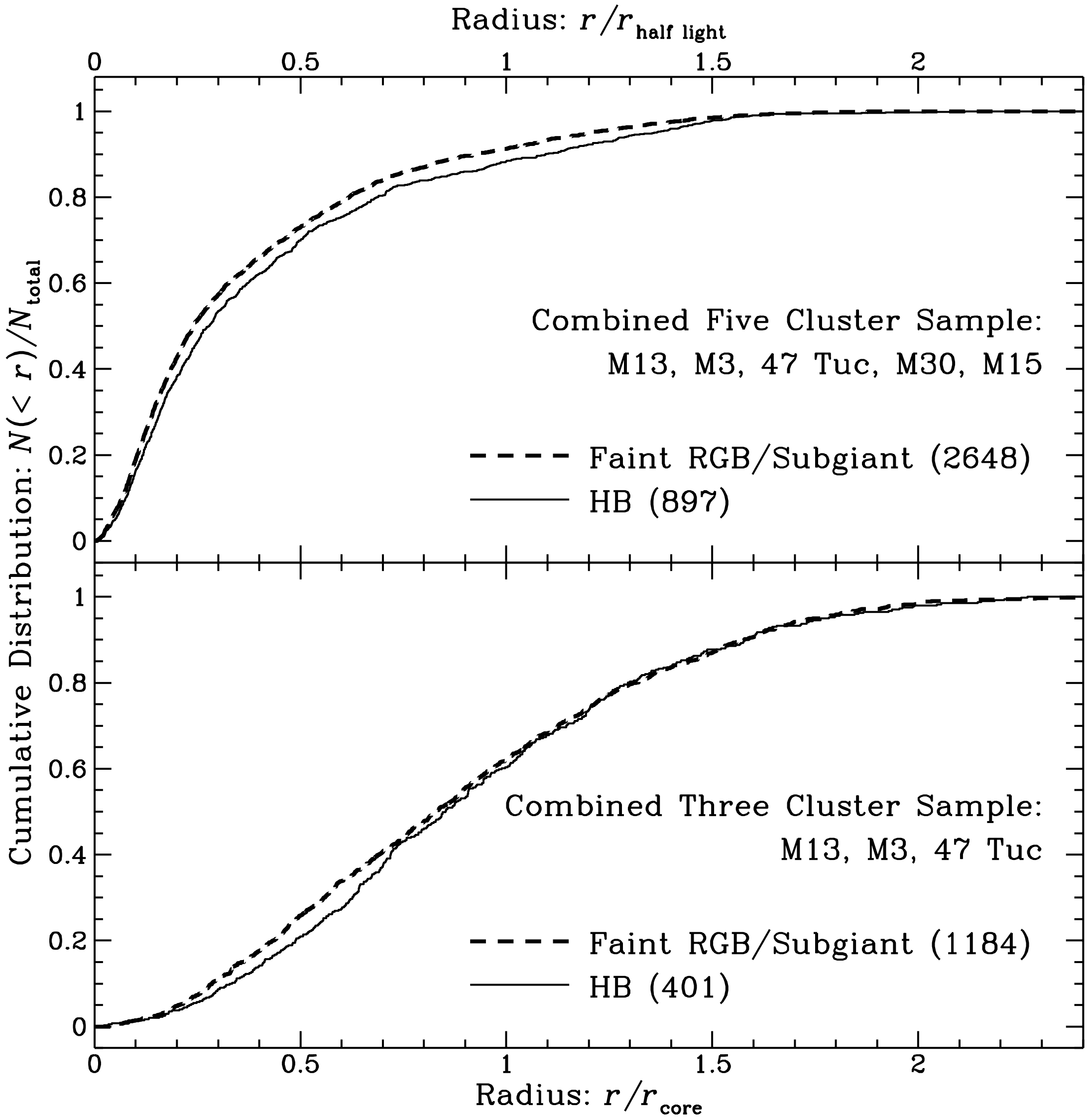

Fig. 6.— The cumulative radial distribution of HB stars (solid line) compared to that of faint RGB/subgiant stars (dashed line) in combined samples of globular clusters. The number of stars in each category is shown within parentheses. **Top:** Combined data from M13, M3, 47 Tuc, M30, and M15, with the projected radius normalized by the half light radius. The HB stars are less centrally concentrated than the giants at the 97% ($\sim 2\sigma$) significance level. **Bottom:** Combined data from only the three King model clusters, M13, M3, and 47 Tuc, with the projected radius normalized by the core radius. The HB stars are less centrally concentrated than the giants at only the 85% ($\sim 1.5\sigma$) significance level.

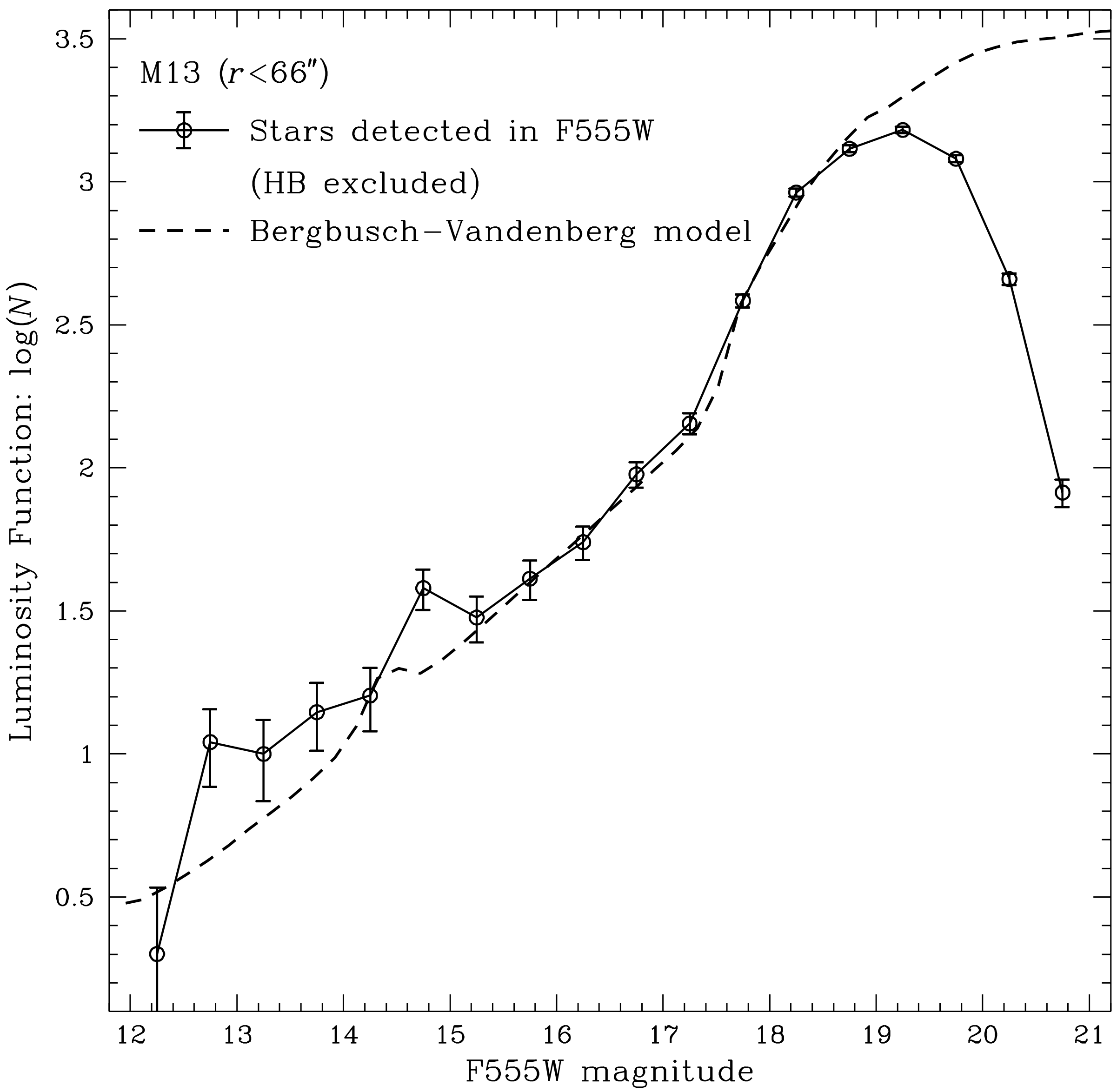

Fig. 7.— The observed stellar luminosity function of M13 (points) compared to the Bergbusch & Vandenberg (1992) model for an old, metal-poor population (dashed line), corrected for the distance modulus and line-of-sight extinction of M13. The error bars indicate the 1σ Poisson error in 0.5 mag bins. The model is normalized to the observed number of stars with F555W = 19, adjusted for 90% completeness. It is a good match to the shape of M13's LF over the range F555W $\approx$ 15–18.5, beyond which the M13 sample is incomplete. Note the significant excess of bright RGB stars (F555W $\approx$ 12.5–15) in M13 relative to the model.